Hindawi
International Journal of Antennas and Propagation
Volume 2019, Article ID 8691903, 16 pages
https://doi.org/10.1155/2019/8691903

Research Article

Radar Coherent Detection for Maneuvering Target Based on Product-Scaled Integrated Cubic Phase Function

Jinyang Chen,[1,2] **Ke Jin**,[1] **Shangjiang Yu**,[2] **Tao Lai**,[3] **and Yongjun Zhao**[1]

[1]*PLA Strategic Support Force Information Engineering University, Zhengzhou 450001, China*
[2]*Institute of Defense Engineering, Academy of Military Sciences, PLA, Luoyang 471000, China*
[3]*School of Electronics and Communication Engineering, Sun Yat-Sen University, Guangzhou 510000, China*

Correspondence should be addressed to Jinyang Chen; chenjinyang_xd@outlook.com

Received 7 August 2019; Revised 11 October 2019; Accepted 14 November 2019; Published 5 December 2019

Academic Editor: Stefania Bonafoni

This paper considers the long-time coherent detection problem for maneuvering targets with jerk motion. A novel method based on product-scaled integrated cubic phase function (PSICPF) is proposed. The main strategy of PSICPF is to estimate target's motion parameters along the slow time for each range frequency cell. In order to eliminate the coupling terms between range frequency and slow time, the scaled nonuniform fast Fourier transform (SNUFFT) is newly defined in the integrated cubic phase function (ICPF). Then, the product operation is employed to coherently synthesize the estimation results, improve the antinoise performance, and suppress the cross terms. Finally, coherent integration is achieved via keystone transform (KT) and fold factor searching. Analysis demonstrates that the SNUFFT has the same computational complexity with nonuniform fast Fourier transform (NUFFT), and thus the PSICPF could be efficiently implemented via complex multiplications, the fast Fourier transform (FFT), and NUFFT. Detailed comparisons with other representative methods in computational cost, motion parameter estimation performance, and detection ability indicate that the PSICPF could achieve a good balance between the computational cost and detection ability. Simulations and real data processing results are presented to verify the effectiveness of the proposed method.

1. Introduction

The illegal flight activities of unmanned aerial vehicle (UAV) have caused great danger to air safety [1]. Therefore, radar maneuvering target detection attracts increasing attention in recent years. In order to detect such low radar cross section (RCS) targets, a long-time coherent integration is always required [2–8]. Unfortunately, the problems that come with it include not only the linear range migration (LRM) caused by the target's high speed [9, 10] but also the range curvature and Doppler frequency migration (DFM) caused by the acceleration and jerk [11–13]. These unfavorable effects seriously deteriorate detection performance of the conventional integration method, e.g., moving target detection (MTD). Consequently, how to effectively detect maneuvering targets is becoming a hot topic in the field of radar signal processing.

In order to coherently detect the targets, many successful methods have been proposed. In summary, these works could be divided into three categories according to the target's maneuverability:

(a) The first category mainly focuses on the LRM caused by the high speed. Representative methods include the keystone transform (KT) [14–16], Radon–Fourier transform (RFT) [17–19], scaled inverse Fourier transform (SCIFT) [20], frequency-domain deramp-keystone transform (FDDKT) [21], axis rotation MTD (AR-MTD) [10], and modified location rotation transform (MLRT) [22]. Nevertheless, due to ignoring the acceleration and jerk, the signal energy will be dispersed in the Doppler domain.

(b) The second category further considers the uniform radial acceleration in the motion. Several typical algorithms could achieve satisfactory integration performance, such as the KT-Dechirp method [23], KT and Lv's distribution (KT-LVD) [24], improved axis

rotation and fractional Fourier transform (IAR-FRFT) [25], KT and linear canonical transform (KT-LCT) [26], MLRT-LVD [27], minimum entropy and Radon transform [28], Radon-LVD (RLVD) [29, 30], RFT-KT [31], frequency-domain second-order phase difference (FD-SoPD) [32], segmented KT and Doppler Lv's transform (SKT-DLVT) [33], frequency autocorrelation function and and Lv's distribution (FAF-LVD) [34], and RFT-FRFT [35]. However, for highly maneuvering targets, jerk motion usually exists and defocuses the Doppler spectrum.

(c) The last category considers the jerk and thus has wider applications. The generalized RFT (GRFT) is proposed as an optimal estimator and detector by multidimensional parameter searching [36]. Despite its perfect detection performance, the serious blind speed side lobes (BSSLs) and huge computational burden prevent its applications. The subband dual-frequency conjugate (SDFC) and Radon-chirp rate-quadratic chirp rate (RCR-QCR), i.e., SRQ method proposed in [37], avoid the BSSLs of GRFT and could estimate motion parameters at low SNR. However, its computational complexity is heavier than GRFT and thus is not suitable for real-time processing. The adjacent cross-correlation function (ACCF) is proposed in [38, 39], which corrects the range migration and DFM by the rank reduction operation. Although the ACCF-based methods have low computational cost, their poor antinoise performance becomes a shortcoming that cannot be ignored. The method based on time reversing transform, second-order KT, and LVD (TRT-SKT-LVD) is proposed in [40]. Similar to the ACCF, the TRT operation obtains high efficiency at the cost of sacrificing the detection performance. In [41], two methods, i.e., KT and generalized dechirp process (KT-GDP) and KT and cubic phase function (KT-CPF), are presented to remove DFM and realize coherent integration. However, the incoherent integration in fold factor searching is sensitive to noise, which limits the detection performance.

This paper extends our preliminary works in [32, 34]. We propose a method based on product-scaled integrated cubic phase function (PSICPF) to achieve coherent detection for maneuvering targets with jerk motion. Different from conventional methods, the main strategy of PSICPF is to estimate motion parameters in the range frequency and slow time domain. The scaling property and product operation are introduced to realize decoupling and energy accumulation. Furthermore, the proposed method could be efficiently implemented via complex multiplications, fast Fourier transform (FFT), and nonuniform FFT (NUFFT) [42]. Detailed comparisons with other representative algorithms indicate that the proposed method could achieve a balance between detection performance and computational cost.

The remainder of this paper is organized as follows: in Section 2, the signal model for a maneuvering target with jerk motion is established. The proposed method is illustrated in detail in Section 3. In Section 4, the properties are analyzed. Experiments with the synthetic and raw data are performed in Section 5 to validate the effectiveness of the proposed method. Finally, Section 6 gives the conclusions.

2. Signal Model and Problem Formulation

Suppose the radar transmits a linear frequency-modulated (LFM) signal, which could be expressed as

$$s_t(\hat{t}) = \mathrm{rect}\left(\frac{\hat{t}}{T_p}\right)\exp\left(j2\pi f_c\hat{t} + j\pi k_r\hat{t}^2\right), \tag{1}$$

where

$$\mathrm{rect}\left(\frac{\hat{t}}{T_p}\right) = \begin{cases} 1, & |\hat{t}| \le \dfrac{T_p}{2}, \\ 0, & |\hat{t}| > \dfrac{T_p}{2}, \end{cases} \tag{2}$$

is the rectangular window function and $\hat{t}$ is the fast time. T_p and f_c indicate, respectively, the pulse width and carrier frequency. $k_r = B/T_p$ is the chirp rate, with B the bandwidth of radar signal.

In most applications, a three-order polynomial could be used to approximate the instantaneous slant range between the maneuvering target and radar; i.e.,

$$R(t_m) \approx R_0 + vt_m + \frac{1}{2}at_m^2 + \frac{1}{6}gt_m^3, \tag{3}$$

where R_0, v, a, and g denote, respectively, the initial slant range, radial velocity, radial acceleration, and jerk of the target. $t_m = mT_m\,(m = 1, 2, \ldots, M)$ denotes the slow time variable, T_m represents the pulse repetition time, and M is the number of integrated pulses.

Ignoring the influence of noise, the received signal after pulse compression can be written as [34]

$$s_c(\hat{t}, t_m) = A_{\mathrm{pc}}\sin c\left[B\left(\hat{t} - \frac{2R(t_m)}{c}\right)\right]\exp\left(-j\frac{4\pi f_c R(t_m)}{c}\right), \tag{4}$$

where A_{pc} and c denote the signal amplitude and the light speed, respectively.

Inserting (3) into (4) yields

$$s_c(\hat{t}, t_m) = A_{\mathrm{pc}}\sin c\left[B\left(\hat{t} - \frac{2\left(R_0 + vt_m + at_m^2/2 + gt_m^3/6\right)}{c}\right)\right] \times \exp\left(-j4\pi\frac{R_0 + vt_m + at_m^2/2 + gt_m^3/6}{\lambda}\right), \tag{5}$$

where $\lambda = c/f_c$ is the wavelength.

As can be seen in equation (5), the first term indicates the signal envelope, which changes nonlinearly with the slow time. When the offset during the observation time exceeds the range resolution $\Delta r = c/2B$, range migration would occur. The exponential term indicates the Doppler frequency of the target, which is defined as [34]

$$f_{d,T} = -\frac{2}{\lambda}\frac{\mathrm{d}\left(R_0 + vt_m + at_m^2/2 + gt_m^3/6\right)}{\mathrm{d}t_m} = -\frac{2\left(v + at_m + gt_m^2/2\right)}{\lambda}. \tag{6}$$

Due to the acceleration and jerk, the Doppler frequency changes nonlinearly with the slow time, which forms a quadratic frequency-modulated (QFM) signal. When the offset exceeds a Doppler resolution, the DFM would occur and seriously defocus the target energy in the Doppler domain.

Performing the Fourier transform (FT) on equation (5) along the $\widehat{t}$-axis, we obtain the compressed signal in the slow time-range frequency domain; i.e.,

$$\begin{aligned} S(f_r, t_m) &= A_f \mathrm{rect}\left(\frac{f_r}{B}\right)\exp\left[-j\frac{4\pi(f_r+f_c)R(t_m)}{c}\right] \\ &= A_f \mathrm{rect}\left(\frac{f_r}{B}\right)\exp \\ &\quad \cdot\left[-j4\pi\frac{(f_r+f_c)(R_0+vt_m+at_m^2/2+gt_m^3/6)}{c}\right], \end{aligned} \tag{7}$$

where A_f is the amplitude of the spectrum and f_r denotes the range frequency variable.

It is obvious in equation (7) that the coupling between f_r and t_m is the essential cause of range migration. In order to detect the maneuvering target in low SNR background, the coupling terms and DFM should be eliminated correctly by an effective detection method.

3. Principle of the Proposed Method

In conventional methods, the range migration is firstly corrected in the slow-range time domain, and then the DFM is estimated and eliminated. However, in our proposed method, the PSICPF is derived in range frequency-slow time domain to estimate the acceleration and jerk. Then, the KT and fold factor searching are employed to achieve coherent integration.

3.1. Parameter Estimation via PSICPF. In equation (7), the signal along the slow time could be expressed as

$$S(t_m; f_r) = A_f \mathrm{rect}\left(\frac{f_r}{B}\right)\exp\left[j2\pi\xi\frac{(\varphi_0+\varphi_1 t_m+\varphi_2 t_m^2)}{2}+\frac{(\varphi_3 t_m^3)}{6}\right], \tag{8}$$

where $\xi = (f_r + f_c)/f_c$ is the scaling factor dependent on the range frequency and $\varphi_0 = -2R_0/\lambda$, $\varphi_1 = -2v/\lambda$, $\varphi_2 = -2a/\lambda$, and $\varphi_3 = -2g/\lambda$ denote the constant phase, centroid frequency, chirp rate, and quadratic chirp rate, respectively.

The cubic phase function (CPF) [43] is defined as a bilinear autocorrelation operation over the slow time; i.e.,

$$\begin{aligned} R_s(t_m, \tau_m; f_r) &= S(t_m+\tau_m; f_r)S(t_m-\tau_m; f_r) \\ &= A_f^2 \mathrm{rect}\left(\frac{f_r}{B}\right)\exp\Big[j4\pi\xi(\varphi_0+\varphi_1 t_m+\varphi_2 t_m^2/2 \\ &\quad +\varphi_3 t_m^3/6)\Big]\times\exp\left[j2\pi\xi(\varphi_2+\varphi_3 t_m)\tau_m^2\right], \end{aligned} \tag{9}$$

where τ_m is the lag variable.

In [44], the NUFFT is performed with respect to τ_m^2 to accumulate the signal energy; i.e.,

$$\begin{aligned} G_{\mathrm{NU}}\left(t_m, f_{\tau_m^2}; f_r\right) &= \mathrm{NUFFT}_{\tau_m^2}\left[R_s(t_m, \tau_m; f_r)\right] \\ &= \int_{\tau_m^2} R_s(t_m, \tau_m)\exp\left(-j2\pi f_{\tau_m^2}\tau_m^2\right)\mathrm{d}\tau_m^2 \\ &= A_f^2 \mathrm{rect}\left(\frac{f_r}{B}\right)\exp \\ &\quad \cdot\left[j4\pi\xi\left(\varphi_0+\varphi_1 t_m+\frac{\varphi_2 t_m^2}{2}+\frac{\varphi_3 t_m^3}{6}\right)\right] \\ &\quad \times\delta\left(f_{\tau_m^2}-\xi\varphi_2-\xi\varphi_3 t_m\right), \end{aligned} \tag{10}$$

where $f_{\tau_m^2}$ is the frequency variable corresponding to τ_m^2 and $\delta(\cdot)$ is the Dirac delta function.

In equation (10), the signal energy peaks along the inclined line $f_{\tau_m^2} = \xi\varphi_2 + \xi\varphi_3 t_m$. However, because of the coupling between f_r and t_m, the interception and slope of this line indicate the wrong values. Therefore, we consider the scaling factor ξ and propose the scaled NUFFT (SNUFFT), which could be written as

$$\begin{aligned} G_{\mathrm{SNU}}\left(t_m, f'_{\tau_m^2}; f_r\right) &= \mathrm{SNUFFT}_{\tau_m^2}\left[R_s(t_m, \tau_m; f_r)\right] \\ &= \int_{\xi\tau_m^2} R_s(t_m, \tau_m)\exp\left(-j2\pi\xi f'_{\tau_m^2}\tau_m^2\right)d\xi\,\tau_m^2 \\ &= A_f^2 \mathrm{rect}\left(\frac{f_r}{B}\right)\exp \\ &\quad \cdot\left[j4\pi\xi\left(\varphi_0+\varphi_1 t_m+\frac{\varphi_2 t_m^2}{2}+\frac{\varphi_3 t_m^3}{6}\right)\right] \\ &\quad \times\delta\left(f'_{\tau_m^2}-\varphi_2-\varphi_3 t_m\right), \end{aligned} \tag{11}$$

where $f'_{\tau_m^2}$ is the scaled frequency variable corresponding to $\xi\tau_m^2$.

Different from NUFFT, the peak position is corrected to the right place after SNUFFT. In this case, the parameter estimation result will keep consistent for all range frequency cells, which benefits to the coherent integration of signal energy. At the same time, the SNUFFT could also be efficiently implemented via NUFFT without increasing the computational burden.

In equation (9), the slow time t_m and lag variable τ_m^2 are coupled with each other, which is the essential cause of the inclined line. Different from the LVD [30], the first exponential term in equation (11) makes difficulties in the decoupling process. In the integrated CPF (ICPF) [45], the complex modulus and inverse FT (IFT) are performed to eliminate the disturbance of $\exp[j4\pi\xi(\varphi_0+\varphi_1 t_m+\varphi_2 t_m^2/2+\varphi_3 t_m^3/6)]$; i.e.,

$$Q(t_m, p_m; f) = \mathrm{IFT}_{f'_{\tau_m^2}}\left[\left|G_{\mathrm{SNU}}\left(t_m, f'_{\tau_m^2}; f_r\right)\right|\right] \approx A_f^2 \mathrm{rect}\left(\frac{f_r}{B}\right)\exp\left[j2\pi(\varphi_2 + \varphi_3 t_m)p_m\right], \tag{12}$$

where p_m is the time variable with respect to $f'_{\tau_m^2}$.

Finally, the scaled Fourier transform (SFT) [46] and FT are employed to coherently integrate the signal energy in the chirp rate-quadratic chirp rate (CR-QCR) domain:

$$D\left(f_{\mathrm{cr}}, f_{\mathrm{qcr}}; f_r\right) = \mathrm{FT}_{p_m}\cdot\left[\int_{t_m} Q(t_m, p_m; f_r)\exp\left(-j2\pi f_{\mathrm{qcr}} t_m p_m\right)dt_m\right] = A_f^2 \mathrm{rect}\left(\frac{f_r}{B}\right)\delta(f_{\mathrm{cr}} - \varphi_2)\delta\left(f_{\mathrm{qcr}} - \varphi_3\right). \tag{13}$$

As can be seen from equation (13), the signal is accumulated into a peak, of which the position is (φ_2, φ_3). For different range frequency cells, the peak locates at the same position. In order to improve the antinoise performance of parameter estimation and suppress the side lobes, the product operation could be employed over the range frequency. In this case, the PSICPF is defined, which coherently integrates the signal energy as

$$P\left(f_{\mathrm{cr}}, f_{\mathrm{qcr}}\right) = \prod_{f_r=-B/2}^{B/2} D\left(f_{\mathrm{cr}}, f_{\mathrm{qcr}}; f_r\right) = A_p\delta(f_{\mathrm{cr}} - \varphi_2)\delta\left(f_{\mathrm{qcr}} - \varphi_3\right), \tag{14}$$

where A_p is the amplitude after product.

By equation (14), we could simultaneously estimate the chirp rate and quadratic chirp rate from the peak position; i.e.,

$$\left(f_{\mathrm{cr,max}}, f_{\mathrm{qcr,max}}\right) = \arg\max_{f_{\mathrm{cr}}, f_{\mathrm{qcr}}}\left|P\left(f_{\mathrm{cr}}, f_{\mathrm{qcr}}\right)\right|. \tag{15}$$

Finally, the acceleration and jerk of the target are derived as

$$\widehat{a} = -\frac{\lambda f_{\mathrm{cr,max}}}{2}, \qquad \widehat{g} = -\frac{\lambda f_{\mathrm{qcr,max}}}{2}. \tag{16}$$

3.2. Coherent Integration via KT. Referring to equation (7), we may utilize the estimated parameters to construct the following phase compensation function to compensate the range curvature and DFM caused by acceleration and jerk:

$$H_{\mathrm{com},1}(f_r, t_m) = \exp\left[j4\pi(f_r + f_c)\frac{\widehat{a}t_m^2/2 + \widehat{g}t_m^3/6}{c}\right]. \tag{17}$$

Multiplying equation (17) by equation (7), we have

$$S_{\mathrm{com},1}(f_r, t_m) = S(f_r, t_m)\cdot H_{\mathrm{com},1}(f_r, t_m) = A_f \mathrm{rect}\left(\frac{f_r}{B}\right)\exp\left[-j4\pi(f_r + f_c)\frac{R_0 + vt_m}{c}\right]. \tag{18}$$

The expression in equation (18) shows that the effects of acceleration and jerk are removed and only the linear coupling term caused by the target velocity exists. However, due to the high speed of target and the low-pulse repetition frequency (PRF) of radar, Doppler ambiguity would often occur. In this case, the velocity of the target can be stated as

$$v = n_b v_b + v_0, \tag{19}$$

where n_b is the ambiguity integer named the fold factor, $v_b = \lambda f_p/2$ is the blind speed with $f_p = 1/T_m$ the PRF, $v_0 = \mathrm{mod}(v, v_b)$ denotes the ambiguous velocity which satisfies $|v_0| < v_b/2$, and $\mathrm{mod}(\cdot)$ is the remainder function.

Substituting equation (19) into equation (18), we obtain

$$S_{\mathrm{com},1}(f_r, t_m) = A_f \mathrm{rect}\left(\frac{f_r}{B}\right)\exp\left(-j4\pi\frac{R_0 + v_0 t_m}{\lambda}\right)\times \exp\left(-j4\pi f_r\frac{R_0 + v_0 t_m + n_b v_b t_m}{c}\right), \tag{20}$$

where the fact $\exp(-j4\pi n_b v_b t_m/\lambda) = 1$ is used.

To achieve coherent integration, many successful methods have been proposed [14–16]. In this paper, the KT is employed for convenience, which scales the slow time for each range frequency:

$$t_m = \frac{f_c}{f_r + f_c}t_a. \tag{21}$$

Substituting the scaling formula into (20), we get

$$S_{\mathrm{KT}}(f_r, t_m) = A_f \mathrm{rect}\left(\frac{f_r}{B}\right)\exp\left(-j4\pi\frac{R_0 + v_0 t_m}{\lambda}\right)\times \exp\left(-j4\pi f_r\frac{R_0 + n_b v_b t_m}{c}\right). \tag{22}$$

By equation (22), the coupling caused by the ambiguous velocity is removed. However, the residual range migration caused by integral multiples of blind speed, i.e., the coupling between $n_b v_b$ and t_m, is still present. Thus, another phase compensation function is established to search the unknown fold factor and then to achieve coherent integration; i.e.,

$$H_{\mathrm{com},2}(f_r, t_m; n_s) = \exp\left[j4\pi f_r\frac{n_s v_b t_m}{c}\right], \tag{23}$$

where n_s is the searching fold factor.

Multiplying (23) with (22) and performing IFT along the range frequency, we may obtain

$$s_c(\widehat{t}, t_m; n_s) = \mathrm{IFT}_{f_r}\left[S_{\mathrm{KT}}(f_r, t_m)\cdot H_{\mathrm{com},2}(f_r, t_m; n_s)\right] = A_{\mathrm{pc}}\sin c\left[B\left(\widehat{t} - \frac{2R_0}{c} - \frac{2(n_b - n_s)v_b t_m}{c}\right)\right]\cdot \exp\left(-j\frac{4\pi v_0 t_m}{\lambda}\right). \tag{24}$$

When $n_b = n_s$, the range migration will be eliminated and the FT could be performed with respect to the slow time to achieve coherent integration; i.e.,

$$E(\hat{t}, f_d; n_s = n_b) = A_{\mathrm{pc}} \sin c\left[B\left(\hat{t} - \frac{2R_0}{c}\right)\right] \sin c\left[\mathrm{MT}_m\left(f_d + \frac{2v_0}{\lambda}\right)\right]. \tag{25}$$

The searching fold factor could be estimated by comparing the amplitude of $E(\hat{t}, f_d; n_s)$:

$$\hat{n}_b = \arg\max_{n_s}\left[\left|E(\hat{t}, f_d; n_s)\right|\right]. \tag{26}$$

Finally, the target velocity is estimated as

$$\begin{cases} \hat{v}_0 = -\dfrac{\lambda f_{d,\max}}{2}, \\ \hat{v} = \hat{n}_b v_b + \hat{v}_0. \end{cases} \tag{27}$$

In (25), the received signal of a maneuvering target is integrated into a single peak with the peak value $|E(\hat{t}, f_d; n_s = n_b)|$. Thereafter, the constant false alarm rate (CFAR) technique could be used for target detection; i.e.,

$$\left|E(\hat{t}, f_d; n_s = n_b)\right| \underset{H_0}{\overset{H_1}{\lessgtr}} \eta, \tag{28}$$

where η is the detection threshold. The adaptive threshold is obtained by the reference unit after coherent integration via the integration method, and then the test statistic in the detecting unit is compared with the threshold to confirm the presence or absence of a target. If the test statistic is smaller than the threshold, there will be no moving target or a target is missed, and then it moves on to the next detecting unit. Meanwhile, if the test statistic is larger than the threshold, the target detection is declared.

4. Analysis of the Proposed Method

4.1. Cross Terms Analysis. Similar to (7), the received signal of K targets in range frequency domain could be written as

$$S(f_r, t_m) = \sum_{k=1}^{K} A_{f,k}\mathrm{rect}\left(\frac{f_r}{B}\right)\exp \cdot \left[-j4\pi(f_r + f_c)\frac{R_{0,k} + v_k t_m + a_k t_m^2/2 + g_k t_m^2/6}{c}\right]. \tag{29}$$

The cubic phase function of (29) is

$$\begin{aligned} R_s(t_m, \tau_m; f_r) &= S(t_m + \tau_m; f_r) S(t_m - \tau_m; f_r) \\ &= R_{\mathrm{auto}}(t_m, \tau_m; f_r) + R_{\mathrm{cros1}}(t_m, \tau_m; f_r) \\ &\quad + R_{\mathrm{cros2}}(t_m, \tau_m; f_r), \end{aligned} \tag{30}$$

where

$$R_{\mathrm{auto}}(t_m, \tau_m; f_r) = \sum_{k=1}^{K} A_{f,k}^2 \mathrm{rect}\left(\frac{f_r}{B}\right)\exp \cdot \left[j2\pi\xi\left(\varphi_{2,k} + \varphi_{3,k} t_m\right)\tau_m^2\right] \times \exp \cdot \left[j4\pi\xi\frac{\left(\varphi_{0,k} + \varphi_{1,k} t_m + \varphi_{2,k} t_m^2\right)}{2} + \frac{\left(\varphi_{3,k} t_m^3\right)}{6}\right], \tag{31}$$

are the self-terms, and

$$\begin{aligned} &R_{\mathrm{cros1}}(t_m, \tau_m; f_r) \\ &= \sum_{l=1}^{K}\sum_{q=1, q\neq l}^{K} A_{f,l} A_{f,q} \mathrm{rect}\left(\frac{f_r}{B}\right)\exp \\ &\quad \cdot \left\{j2\pi\xi\left[\frac{1}{2}\left(\varphi_{2,l} + \varphi_{2,q}\right) + \frac{1}{2}\left(\varphi_{3,l} + \varphi_{3,q}\right) t_m\right]\tau_m^2\right\} \\ &\quad \times \exp\left\{j2\pi\xi\left[\left(\varphi_{0,l} + \varphi_{0,q}\right) + \left(\varphi_{1,l} + \varphi_{1,q}\right) t_m + \frac{1}{2}\left(\varphi_{2,l} + \varphi_{2,q}\right) t_m^2 + \frac{1}{6}\left(\varphi_{3,l} + \varphi_{3,q}\right) t_m^3\right]\right\} \\ &\quad \times \exp\left\{j2\pi\xi\left[\left(\varphi_{1,l} - \varphi_{1,q}\right)\tau_m + \left(\varphi_{2,l} - \varphi_{2,q}\right) t_m \tau_m + \frac{1}{2}\left(\varphi_{3,l} - \varphi_{3,q}\right) t_m^2 \tau_m + \frac{1}{6}\left(\varphi_{3,l} - \varphi_{3,q}\right)\tau_m^3\right]\right\}, \end{aligned} \tag{32}$$

$$\begin{aligned} &R_{\mathrm{cros2}}(t_m, \tau_m; f_r) \\ &= \sum_{q=1}^{K}\sum_{l=1, l\neq q}^{K} A_{f,q} A_{f,l} \mathrm{rect}\left(\frac{f_r}{B}\right)\exp\left\{j2\pi\xi\left[\frac{1}{2}\left(\varphi_{2,q} + \varphi_{2,l}\right) + \frac{1}{2}\left(\varphi_{3,q} + \varphi_{3,l}\right) t_m\right]\tau_m^2\right\} \\ &\quad \times \exp\left\{j2\pi\xi\left[\left(\varphi_{0,q} + \varphi_{0,l}\right) + \left(\varphi_{1,q} + \varphi_{1,l}\right) t_m + \frac{1}{2}\left(\varphi_{2,q} + \varphi_{2,l}\right) t_m^2 + \frac{1}{6}\left(\varphi_{3,q} + \varphi_{3,l}\right) t_m^3\right]\right\} \\ &\quad \times \exp\left\{j2\pi\xi\left[\left(\varphi_{1,q} - \varphi_{1,l}\right)\tau_m + \left(\varphi_{2,q} - \varphi_{2,l}\right) t_m \tau_m + \frac{1}{2}\left(\varphi_{3,q} - \varphi_{3,l}\right) t_m^2 \tau_m + \frac{1}{6}\left(\varphi_{3,q} - \varphi_{3,l}\right)\tau_m^3\right]\right\}, \end{aligned}$$

are the cross terms.

According to Euler's formula, i.e.,

$$\exp(j\theta) + \exp(-j\theta) = 2\cos\theta, \tag{33}$$

we obtain

$$\begin{aligned} R_{\text{cross}}(t_m, \tau_m; f_r) &= R_{\text{cros1}}(t_m, \tau_m; f_r) + R_{\text{cros2}}(t_m, \tau_m; f_r) \\ &= \sum_{q=1}^{K} \sum_{l=1, l\neq q}^{K} 2A_{f,q}A_{f,l}\,\text{rect}\left(\frac{f_r}{B}\right)\exp\left\{j2\pi\xi\left[\frac{1}{2}(\varphi_{2,q} + \varphi_{2,l}) + \frac{1}{2}(\varphi_{3,q} + \varphi_{3,l})t_m\right]\tau_m^2\right\} \\ &\times \exp\left\{j2\pi\xi\left[(\varphi_{0,q} + \varphi_{0,l}) + (\varphi_{1,q} + \varphi_{1,l})t_m + \frac{1}{2}(\varphi_{2,q} + \varphi_{2,l})t_m^2 + \frac{1}{6}(\varphi_{3,q} + \varphi_{3,l})t_m^3\right]\right\} \\ &\times \cos\left\{2\pi\xi\left[(\varphi_{1,q} - \varphi_{1,l})\tau_m + (\varphi_{2,q} - \varphi_{2,l})t_m\tau_m + \frac{1}{2}(\varphi_{3,q} - \varphi_{3,l})t_m^2\tau_m + \frac{1}{6}(\varphi_{3,q} - \varphi_{3,l})\tau_m^3\right]\right\}. \end{aligned} \tag{34}$$

The cross terms for multiple targets at a certain range frequency cell could be obtained as

$$D_{\text{cross}}(f_{\text{cr}}, f_{\text{qcr}}; f_r) = \text{FT}_{p_m}\left\{\text{SFT}_{p_m t_m}\left\{\text{IFT}_{f'_{\tau_m^2}}\left\{\left|\text{SNUFFT}_{\tau_m^2}[R_{\text{cross}}(t_m, \tau_m; f_r)]\right|\right\}\right\}\right\}. \tag{35}$$

It can be seen from (34) and (35) that the cosine function and the nonlinear coupling terms would disturb the integration of the cross terms after SNUFFT, complex modulus, IFT, and SFT. Only when $\varphi_{1,q} = \varphi_{1,l}$, $\varphi_{2,q} = \varphi_{2,l}$, and $\varphi_{3,q} = \varphi_{3,l}$, the cosine function could be eliminated. In this case, the cross terms become the self-terms. Thus, the cross terms of PSICPF cannot be accumulated.

4.2. Computational Complexity Analysis. In this part, the computational burden of the proposed method is analyzed in detail. The GRFT, KT-GDP, KT-CPF, and TRT-SKT-LVD, which could also complete coherent detection for maneuvering target, are selected for comparisons. Denote the number of range cells, echo pulses, searching velocity, searching acceleration, searching jerk, and searching fold factor as N_r, M, N_v, N_a, N_g, and N_F, respectively.

For GRFT, a four-dimensional parameter searching is needed. The computational complexity can be easily obtained as $O(N_r M N_g N_a N_v)$ [36].

For KT-GDP, the KT and fold factor searching are firstly performed to eliminate the LRM, and the computational costs are, respectively, $O(3N_r M \log_2 M)$ [16] and $O(N_F M N_r \log_2 M N_r)$. The GDP is then employed to estimate the acceleration and jerk, of which the computational cost is at the order of $O(M N_a N_g \log_2 M)$. Therefore, the total computational complexity is about $O(N_F M N_r \log_2 N_r + M N_a N_g \log_2 M)$ [39].

Compared with KT-GDP, the acceleration and jerk are estimated via CPF, of which the computational cost is about $O(2M^2 \log_2 M)$ [44]. In this case, the computational complexity of KT-CPF is about $O(N_F M N_r \log_2 M N_r)$.

For TRT-SKT-LVD, to complete the chirp-z-based SKT and LVD, the computational complexities are $O(3N_r M \log_2 M)$ and $O(3M^2 \log_2 M)$, respectively. Therefore, the total computational complexity is about $O(3(N_r + M)M \log_2 M)$ [40].

For the proposed method, the main procedures in estimating acceleration and jerk for each range frequency bin include the bilinear autocorrelation operation $[O(M^2)]$, the SNUFFT $[O(2M^2 \log_2 M)]$, the IFT along the scaled frequency $[O(M^2 \log_2 M)]$, the SFT with respect to the slow time $[O(3M^2 \log_2 M)]$, and the FT to integrate the signal energy $[O(M^2 \log_2 M)]$. The computational complexity of KT and fold factor are, respectively, $O(4M N_r \log_2 M)$ and $O(N_F M N_r \log_2 M N_r)$. Thus, the total computational complexity is in the order of $O(7N_r M^2 \log_2 M + N_F M N_r \log_2 M N_r)$

The computational complexities of the above methods are listed in Table 1. In practical applications, N_v, N_a, and N_g are usually much larger than M, while N_F is much smaller than M. Under the assumption of $N_r = M$, $N_v = N_a = N_g = N_F M$, and $N_F = 20$, Figure 1 intuitively presents the computational complexities of the above methods. It is obvious that the GRFT and the KT-GDP take too much time due to the multidimensional parameter searching. The proposed method has a moderate computation complexity compared with KT-CPF and TRT-SKT-LVD. However, these two methods have poor detection performance under low SNR environment, which will be shown in Section 5.

Table 1: Computational complexity comparisons of different algorithms.

Method	Computation complexity
GRFT	$O(N_r M N_g N_a N_v)$
KT-CPF	$O(N_F M N_r \log_2 M N_r)$
KT-GDP	$O(N_F M N_r \log_2 M N_r + M N_a N_g \log_2 M)$
TRT-SKT-LVD	$O(3(N_r + M) M \log_2 M)$
Proposed method	$O(7 N_r M^2 \log_2 M + N_F M N_r \log_2 M N_r)$

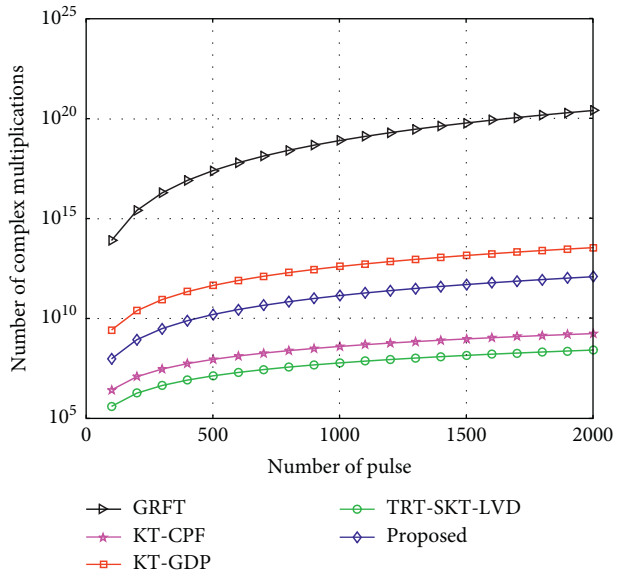

Figure 1: Computational costs of different algorithms.

Table 2: Radar simulation parameters.

Parameters	Value	Parameters	Value
Carrier frequency	1 GHz	Bandwidth	2 MHz
Sample frequency	5 MHz	PRF	512 Hz
Pulse duration	10 μs	Pulse number	1024

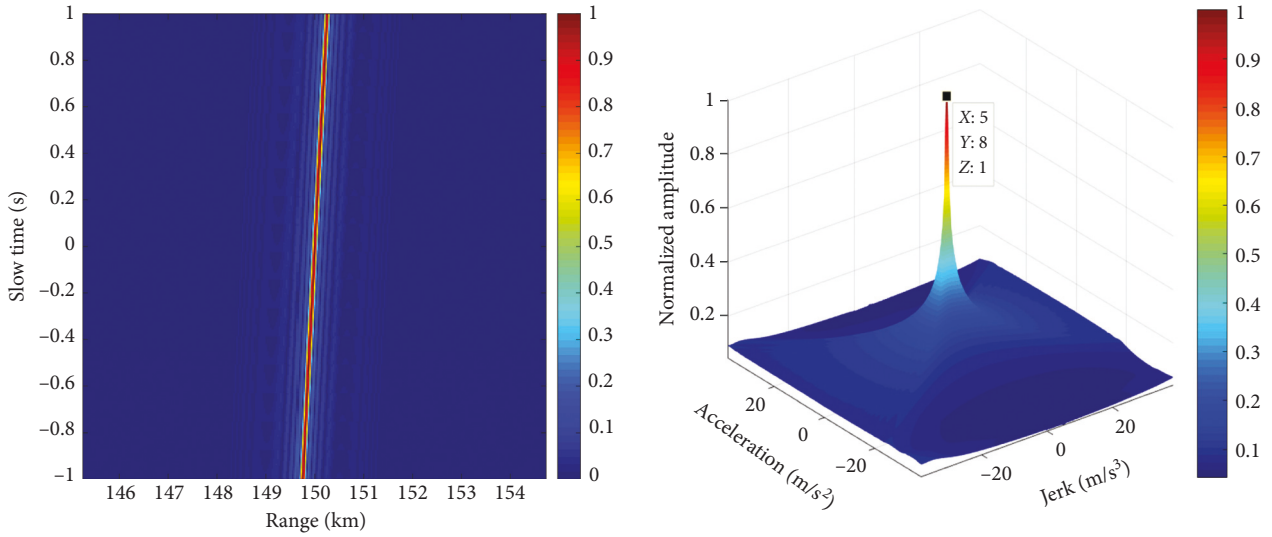

(a) (b)

Figure 2: Continued.

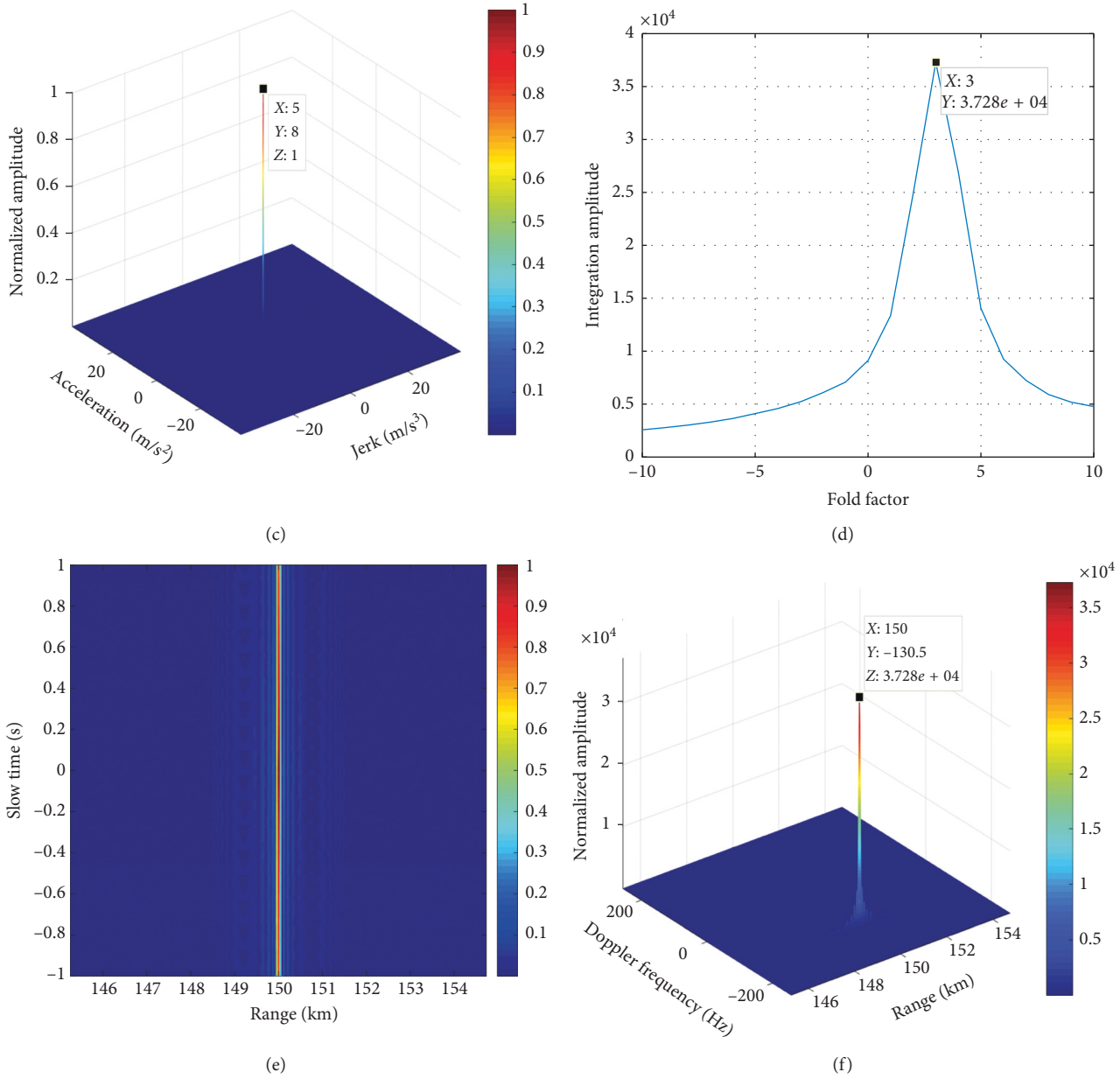

FIGURE 2: Coherent integration for a maneuvering target. (a) Result of pulse compression. (b) Parameter estimation at $f_r = -B/2$. (c) Parameter estimation result of PSICPF. (d) Result of fold factor searching. (e) Result of LRM elimination. (f) Result of coherent integration.

5. Simulations and Real Data Processing Results

In this section, several numerical experiments are given to demonstrate the effectiveness of the proposed method. The simulation parameters are given in Table 2.

5.1. Coherent Integration for a Maneuvering Target. First of all, a single maneuvering target is used to evaluate the coherent integration ability of the proposed method. The motion parameters of the target are $R_0 = 150$ km, $v = 250$ m/s, $a = 8$ m/s^2, and $g = 5$ m/s^3. Figure 2(a) gives the target trajectory. Due to the high speed of the target, serious range migration could be observed. Figure 2(b) shows the parameter estimation result when $f_r = -B/2$. Thanks to the proposed SNUFFT, correct values of acceleration and jerk could be obtained. Then, the PSICPF is achieved by multiplying all the range frequency cells, as presented in Figure 2(c). It is clear that the product operations greatly strengthen the main lobe and suppress the side lobes. From the peak position, we could read that $\hat{a} = 8$ m/s^2 and $\hat{g} = 5$ m/s^3. After compensating for the range migration and DFM caused by acceleration and jerk, the KT and fold factor searching are performed. From Figure 2(d), we could estimate the fold factor, i.e., $\hat{n}_b = 3$. The LRM elimination result is given in Figure 2(e). Finally, coherent integration is

Table 3: Motion parameters of two maneuvering targets.

Target	Amplitude	Initial range (km)	Velocity (m/s)	Acceleration (m/s^2)	Jerk (m/s^3)	SNR (dB)
Tr1	1	150	250	10	6	0
Tr2	1	150.2	−180	−8	−5	0

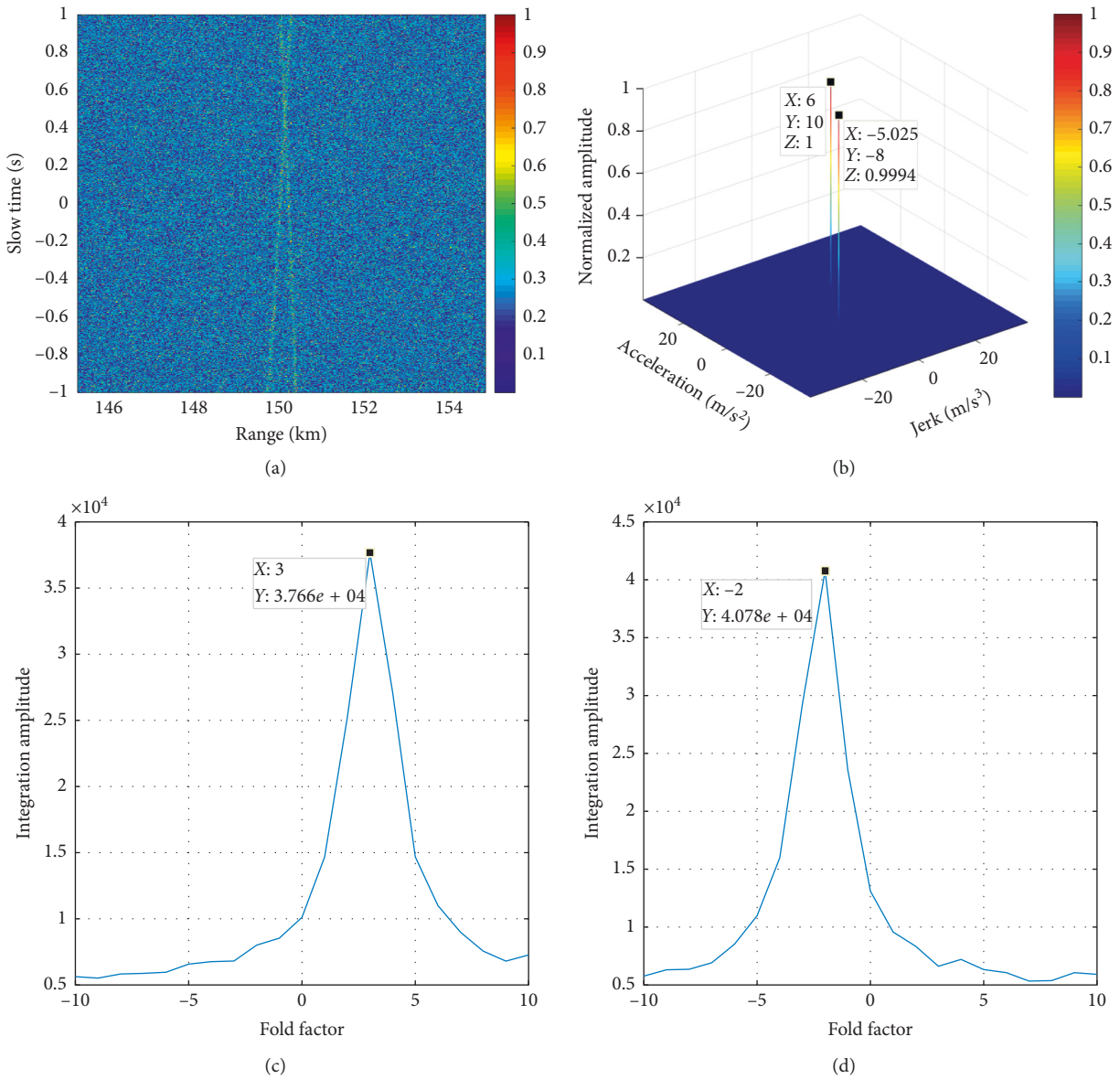

Figure 3: Continued.

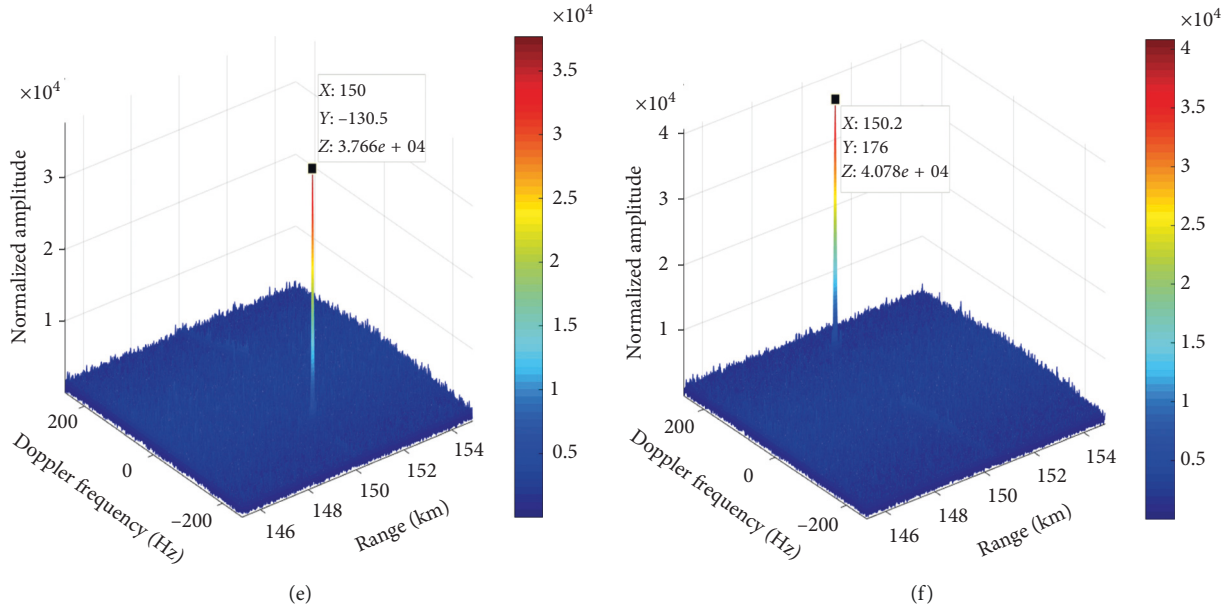

FIGURE 3: Coherent integration for multiple maneuvering targets. (a) Result of pulse compression. (b) Parameter estimation of PSICPF. (c) Result of fold factor searching for Tr1. (d) Result of fold factor searching for Tr2. (e) Coherent integration for Tr1. (f) Coherent integration for Tr2.

realized and a well-focused peak could be seen in the range-Doppler domain, as shown in Figure 2(f). Considering the peak position, we may estimate the target velocity and initial range, i.e., $\widehat{v} = 249.975$ m/s and $\widehat{R}_0 = 150$ km. This experiment preliminarily demonstrates the integration capability of the proposed method.

5.2. Coherent Integration for Multiple Targets. The integration ability of the proposed method for multiple targets (i.e., Tr1 and Tr2) is evaluated in this part, where the motion parameters are listed in Table 3. In this simulation, Gaussian noise with zero mean is added to the signal after pulse compression. The input SNR is defined as

$$\mathrm{SNR} = 10\log_{10}\left(\frac{A_{\mathrm{pc}}^2}{\sigma^2}\right), \tag{36}$$

where σ^2 is the variance of Gaussian noise. Results of integration and parameter estimation are shown in Figure 3.

Figure 3(a) gives the result of range compression. Since the input SNR is 0 dB, the target trajectory could be hardly recognized. Figure 3(b) shows the parameter estimation result of PSICPF. As can be seen, two sharp peaks are obtained in the CR-QCR domain. By product operation, the self-terms are strengthened while the cross terms are greatly suppressed. From the peak position, we get $\widehat{a}_1 = 10\,\mathrm{m/s^2}$ and $\widehat{g}_1 = 6\,\mathrm{m/s^3}$ for Tr1 and $\widehat{a}_2 = -8\,\mathrm{m/s^2}$ and $\widehat{g}_2 = -5.025\,\mathrm{m/s^3}$ for Tr2. After phase compensation with the estimated parameters, the fold factor estimation results are presented in Figures 3(c) and 3(d). For Tr1, we have $\widehat{n}_{b,1} = 3$, and for Tr2, we have $\widehat{n}_{b,2} = -2$. Finally, the coherent integration results are, respectively, given in Figures 3(e) and 3(f). The velocities are estimated as $\widehat{v}_1 = 249.975$ m/s for Tr1 and $\widehat{v}_2 = -180$ m/s.

In Figure 3, the proposed method could achieve coherent integration for multiple targets. In order to intuitively evaluate the impact the cross terms, we could define the normalized cross terms as

$$G_{\mathrm{norm}}\left(f_{\mathrm{cr}}, f_{\mathrm{qcr}}; f_r\right) = \frac{\left|D_{\mathrm{cross}}\left(f_{\mathrm{cr}}, f_{\mathrm{qcr}}; f_r\right)\right|}{\max\left|D_{\mathrm{self}}\left(f_{\mathrm{cr}}, f_{\mathrm{qcr}}; f_r\right)\right|}, \tag{37}$$

where $D_{\mathrm{self}}(f_{\mathrm{cr}}, f_{\mathrm{qcr}}; f_r)$ denotes the self-terms.

The simulation results of cross terms for a certain range frequency cell are shown in Figure 4, where the Gaussian noise is ignored. It is evident that the cross terms show significant oscillation characteristics. The maximum ratio of $G_{\mathrm{norm}}(f_{\mathrm{cr}}, f_{\mathrm{qcr}}; f_r)$ is about 6%. After the product operation of different range frequency cells, the ratio will further decrease. Therefore, we may get the conclusion that the cross terms have little impact on parameter estimation.

5.3. Performance of Target Detection and Parameter Estimation. The detection performance of the proposed method is also evaluated by using the CFAR detector. Complex white Gaussian noise is added to the signal after pulse compression to yield SNRs varying from with −20 dB to 20 dB. 500 independent Monte Carlo trials are performed for each SNR value. The false alarm ratio is set as $P_{\mathrm{fa}} = 10^{-6}$. The representative GRFT, KT-GDP, KT-CPF, and TRT-SKT-LVD are selected for comparisons. The detection performance is given in Figure 5.

First of all, it is important to state that the GRFT has the optimal detection performance since it is designed based on maximum likelihood. Obviously, with the GRFT as a benchmark, the KT-GDP suffers from 6 dB performance loss due to the incoherent procedure in fold

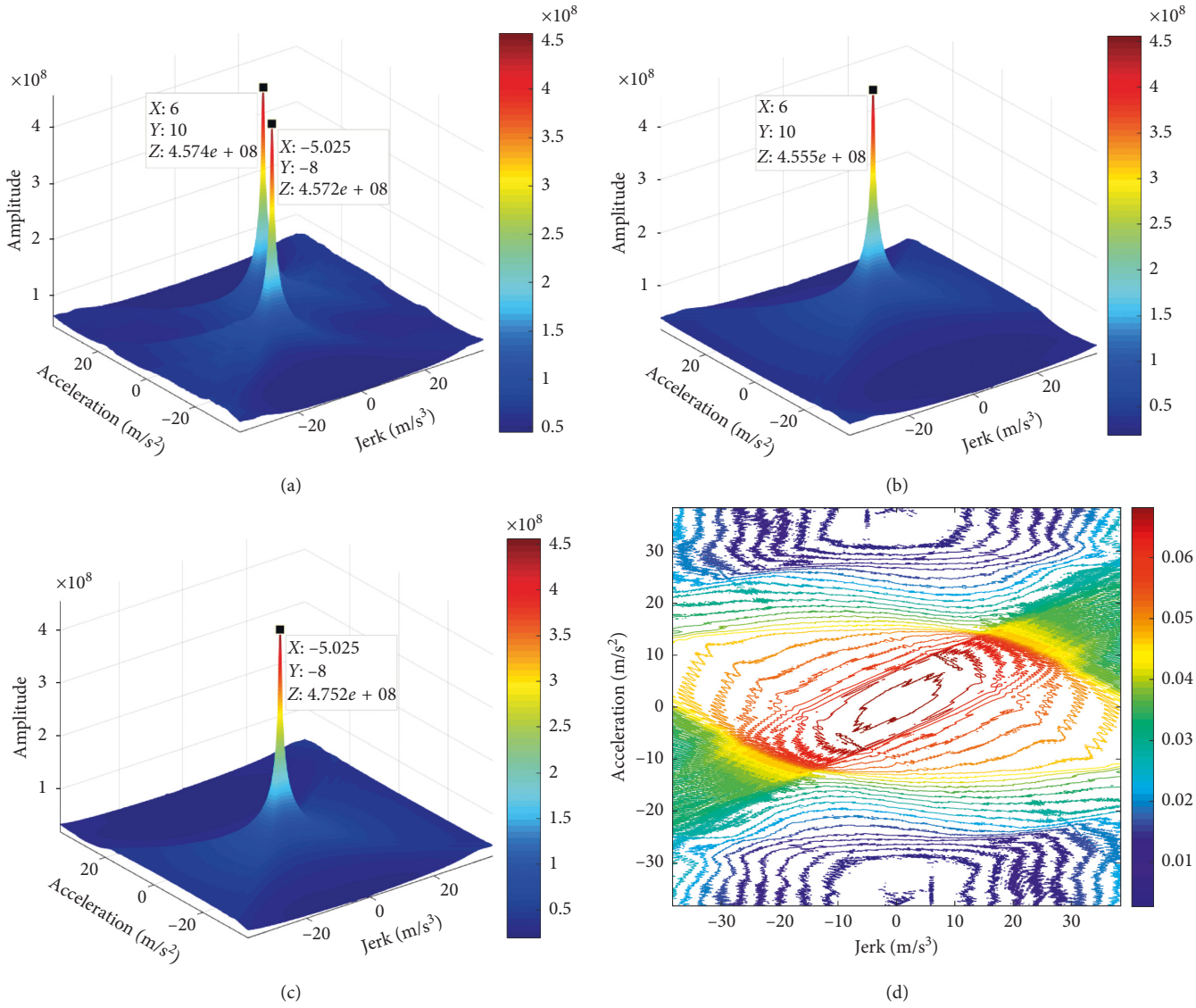

Figure 4: Cross terms of two targets. (a) Parameter estimation result for two targets. (b) Parameter estimation result for Target A. (c) Parameter estimation result for Target B. (d) Contour of the cross terms.

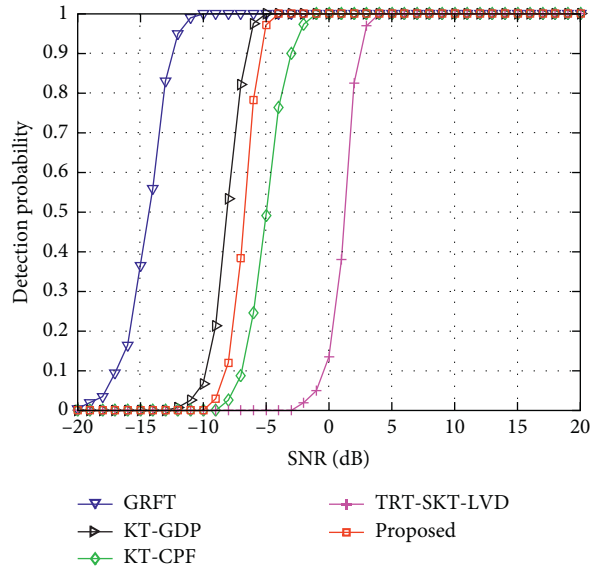

Figure 5: Detection probability of different methods.

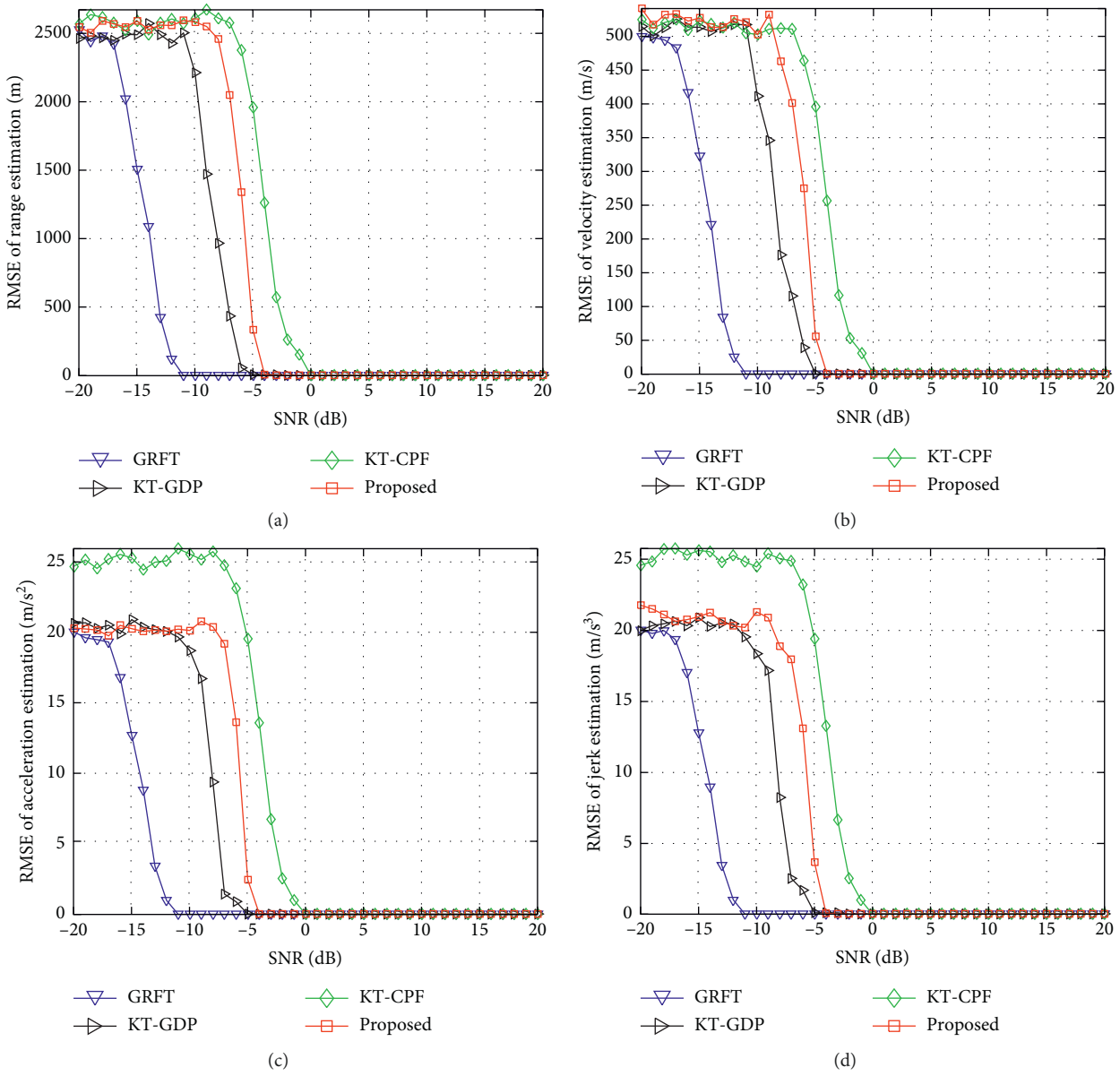

FIGURE 6: Analysis of motion parameter estimation performance. RMSE of (a) initial range estimation, (b) velocity estimation, (c) acceleration estimation, and (d) jerk estimation.

factor searching. The KT-CPF has inferior detection probability at −5 dB than the proposed method since the least squares (LS) method fails at low SNR. The TRT-SKT-LVD is only effective when the SNR is high because the TRT operation loses much signal energy, even though it is beneficial to reducing computational complexity. Therefore, when considering the computational cost, the proposed method is more suitable for practical applications than GRFT.

As the detection performance is determined by the target's acceleration and jerk estimation accuracy, the parameter estimation performance is also evaluated by the experiment. The root-mean-square error (RMSE) is utilized as the criterion. The RMSEs of initial range, velocity, acceleration, and jerk are given in Figures 6(a)–6(d), respectively. Corresponding to the detection performance, the GRFT and KT-GDP have better antinoise performance than the proposed method, and the KT-CPF may get wrong estimation results at low SNR. The TRT-SKT-LVD could not estimate motion parameters and thus is not compared with other methods.

5.4. Real Data Processing Results. In this subsection, we adopt the measured data of a DJI Phantom 3 commercial UAV to demonstrate the proposed method. The data were

(a)

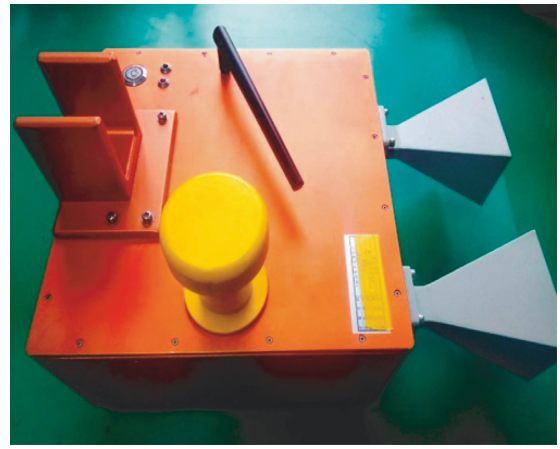

(b)

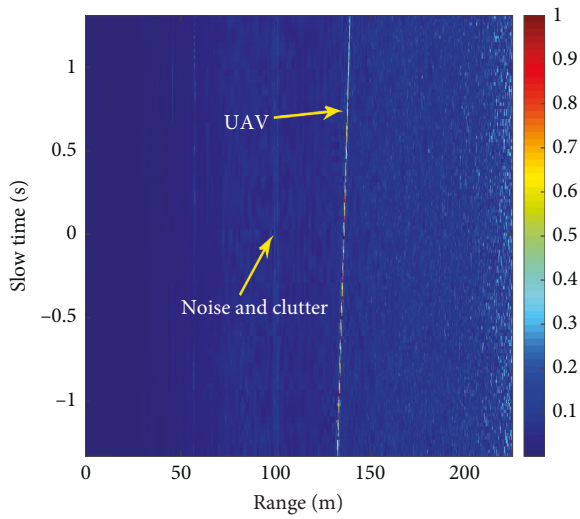

(c)

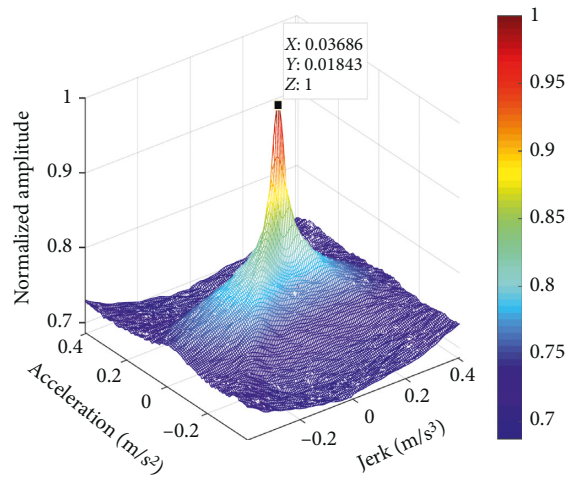

(d)

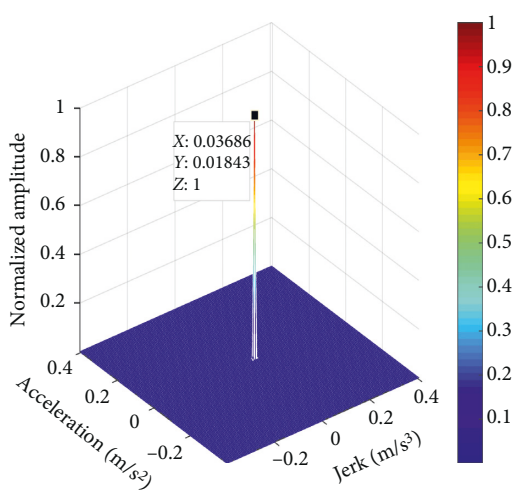

(e)

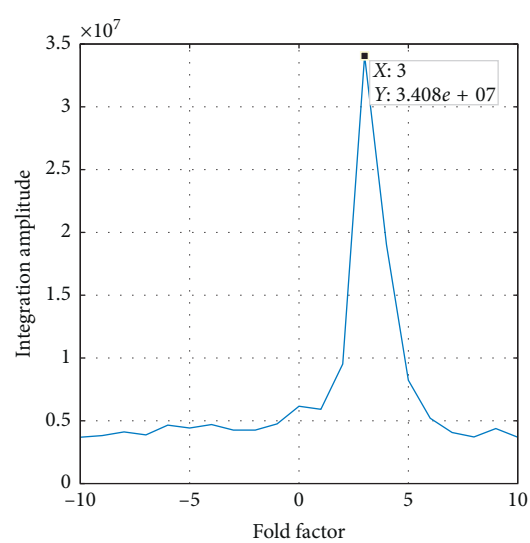

(f)

Figure 7: Continued.

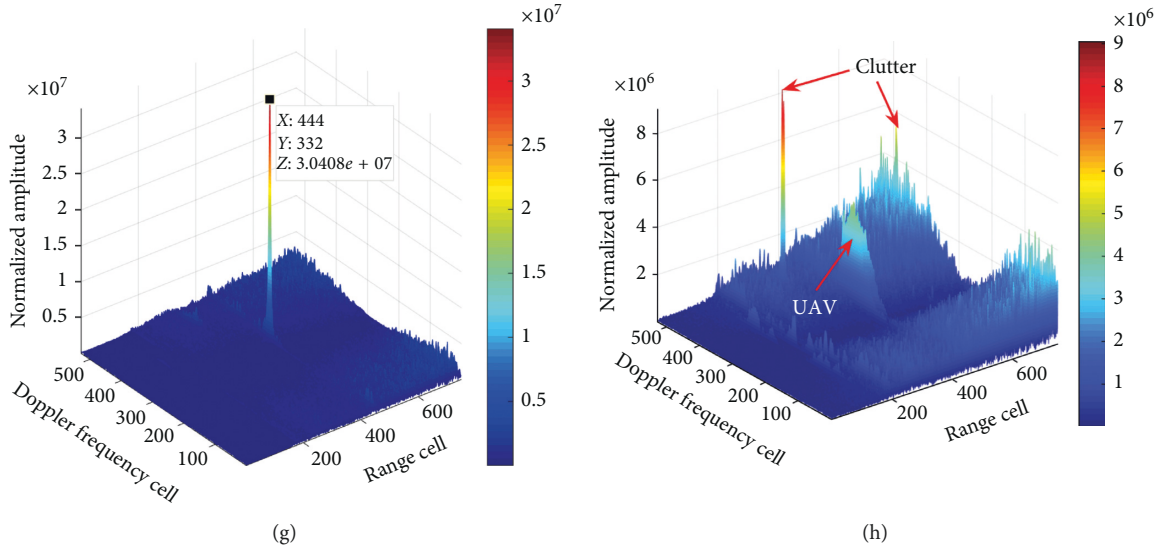

Figure 7: Processing results with real radar data. (a) Experimental scene. (b) FMCW radar system. (c) Result of pulse compression. (d) Parameter estimation at $f_r = -B/2$. (e) Parameter estimation result of PSICPF. (f) Result of fold factor searching. (g) Integration result of the proposed method. (h) Integration result of MTD.

Table 4: FMCW radar parameters.

Radar parameter	Value	Radar parameter	Value
Carrier frequency	9.5 GHz	PRF	50 Hz
Bandwidth	500 MHz	Sampling frequency	1 MHz
Pulse width	0.0102 s	Coherent time	2.64 s

collected in March 2017 by the National University of Defense Technology, Hunan, China. Figures 7(a) and 7(b) present the experimental scene and frequency-modulated continuous wave (FMCW) radar system, respectively. Radar parameters are given in Table 4. It is worth noting that, in order to obtain the LRM and Doppler ambiguity, we deliberately chose a large bandwidth and a low PRF before experiment.

Figure 7(c) shows the target trajectory after pulse compression. During the coherent time, the UAV moves across 24 range cells and causes serious range migration. Figure 7(d) gives the parameter estimation result at $f_r = -0.5$ GHz. From this range frequency, we may obtain the target acceleration and jerk. However, to improve the antinoise performance, the PSICPF is proposed by multiplying all the range frequency cell. Figure 7(e) presents the result of PSICPF, where the noise and clutter are greatly suppressed. The motion parameters of the target are $\widehat{a} = 0.018\,\text{m/s}^2$ and $\widehat{g} = 0.037\,\text{m/s}^3$. Then, the KT and fold factor searching are employed to remove the LRM and achieve coherent integration, of which the results are shown in Figures 7(f) and 7(g), respectively. It is easy to see that a well-focused peak is obtained in the range-Doppler domain. The initial range and velocity of the UAV are $\widehat{R}_0 = 132.9$ m and $\widehat{v} = 2.735$ m/s. At the same time, Figure 7(h) gives the integration result of MTD. Due to ignoring the LRM and DFM effects, the signal energy is dispersed over multiple ranges and Doppler cells, which creates difficulties for target detection. This experiment verifies the practicality of the proposed method.

6. Conclusions and Future Work

In this paper, we have presented a coherent integration method for maneuvering target with jerk motion based on PSICPF. The main strategy of the proposed method is to coherently estimate motion parameters along the slow time for each range frequency. In order to eliminate the coupling between range frequency and slow time, the scaling property is introduced into NUFFT and then the SNUFFT is proposed. When integrating the signal energy, the product operation is applied to improve the antinoise performance and suppress the side lobes. Finally, the KT combining with fold factor searching is performed to achieve coherent integration. The contributions of the proposed method include the following:

(1) The SNUFFT is newly defined to realize decoupling between range frequency and slow time so that the parameter estimation results of different range frequency cells could remain coincident

(2) The product operation is employed to coherently synthesize the estimation results, improve the antinoise performance, and suppress the cross terms

(3) The proposed method could be implemented via complex multiplications, FFT, and NUFFT, which guarantee the high efficiency

(4) The PSICPF achieves a good balance between detection performance and computational complexity

As the bilinear autocorrelation operation in CPF brings about estimation performance loss, linear methods will be considered in the future to further improve the detection ability. The core problem may focus on the efficient implementation.

Data Availability

The radar data used to support the findings of this study are available from the corresponding author upon request.

Conflicts of Interest

The authors declare that there are no conflicts of interest regarding the publication of this paper.

Acknowledgments

This article was supported by the National Natural Science Foundation of China (no. 61501513).

References

[1] X. Li, Z. Sun, T. S. Yeo et al., "STGRFT for detection of maneuvering weak target with multiple motion models," *IEEE Transactions on Signal Processing*, vol. 67, no. 7, pp. 1902–1917, 2019.

[2] P. C. Suo, S. Tao, R. Tao, and Z. Nan, "Detection of high-speed and accelerated target based on the linear frequency modulation radar," *IET Radar Sonar and Navigation*, vol. 8, no. 1, pp. 37–47, 2014.

[3] S. Q. Zhu, G. S. Liao, D. Yang, and H. H. Tao, "A new method for radar high-speed maneuvering weak target detection and imaging," *IEEE Geoscience & Remote Sensing Letters*, vol. 11, no. 7, pp. 1175–1179, 2014.

[4] X. Li, G. Cui, W. Yi, and L. Kong, "Radar maneuvering target detection and motion parameter estimation based on TRT-SGRFT," *Signal Processing*, vol. 133, pp. 107–116, 2017.

[5] W. Wu, G. H. Wang, and J. P. Sun, "Polynomial radon-polynomial Fourier transform for near space hypersonic maneuvering target detection," *IEEE Transactions on Aerospace and Electronic Systems*, vol. 54, no. 3, pp. 1306–1322, 2018.

[6] X. Li, L. Kong, G. Cui, and W. Yi, "CLEAN-based coherent integration method for high-speed multi-targets detection," *IET Radar, Sonar & Navigation*, vol. 10, no. 9, pp. 1671–1682, 2016.

[7] X. Huang, S. Tang, L. Zhang, and S. Li, "Ground-based radar detection for high-speed maneuvering target via fast discrete Chirp-Fourier transform," *IEEE Access*, vol. 7, pp. 12097–12113, 2019.

[8] X. Chen, J. Guan, N. Liu, and Y. He, "Maneuvering target detection via radon-fractional Fourier transform-based long-time coherent integration," *IEEE Transactions on Signal Processing*, vol. 62, no. 4, pp. 939–953, 2014.

[9] Z. Niu, J. Zheng, T. Su, and J. Zhang, "Fast implementation of scaled inverse Fourier transform for high-speed radar target detection," *Electronics Letters*, vol. 53, no. 16, pp. 1142–1144, 2017.

[10] X. Rao, H. Tao, J. Su, X. Guo, and J. Zhang, "Axis rotation MTD algorithm for weak target detection," *Digital Signal Processing*, vol. 26, pp. 81–86, 2014.

[11] J. Zhang, T. Su, J. Zheng, and X. He, "Novel fast coherent detection algorithm for radar maneuvering target with jerk motion," *IEEE Journal of Selected Topics in Applied Earth Observations and Remote Sensing*, vol. 10, no. 5, pp. 1792–1803, 2017.

[12] X. L. Li, Z. Sun, W. Yi, G. L. Cui, L. J. Kong, and X. Yang, "Computationally efficient coherent detection and parameter estimation algorithm for maneuvering target," *Signal Processing*, vol. 155, pp. 130–142, 2018.

[13] X. Li, G. Cui, W. Yi, and L. Kong, "Sequence-reversing transform-based coherent integration for high-speed target detection," *IEEE Transactions on Aerospace and Electronic Systems*, vol. 53, no. 3, pp. 1573–1580, 2017.

[14] R. P. Perry, R. C. DiPietro, and R. L. Fante, "SAR imaging of moving targets," *IEEE Transactions on Aerospace and Electronic Systems*, vol. 35, no. 1, pp. 188–200, 1999.

[15] D. Zhu, Y. Li, and Z. Zhu, "A keystone transform without interpolation for SAR ground moving-target imaging," *IEEE Geoscience and Remote Sensing Letters*, vol. 4, no. 1, pp. 18–22, 2007.

[16] F. Pignol, F. Colone, and T. Martelli, "Lagrange-polynomial-interpolation-based keystone transform for a passive radar," *IEEE Transactions on Aerospace and Electronic Systems*, vol. 54, no. 3, pp. 1151–1167, 2018.

[17] J. Xu, J. Yu, Y.-N. Peng, and X.-G. Xia, "Radon-Fourier transform for radar target detection, I: generalized Doppler filter bank," *IEEE Transactions on Aerospace and Electronic Systems*, vol. 47, no. 2, pp. 1186–1202, 2011.

[18] J. Xu, J. Yu, Y.-N. Peng, and X.-G. Xia, "Radon-Fourier transform for radar target detection (II): blind speed sidelobe suppression," *IEEE Transactions on Aerospace and Electronic Systems*, vol. 47, no. 4, pp. 2473–2489, 2011.

[19] J. Yu, J. Xu, Y.-N. Peng, and X.-G. Xia, "Radon-Fourier transform for radar target detection (III): optimality and fast implementations," *IEEE Transactions on Aerospace and Electronic Systems*, vol. 48, no. 2, pp. 991–1004, 2012.

[20] J. B. Zheng, T. Su, W. T. Zhu, X. H. He, and Q. H. Liu, "Radar high-speed target detection based on the scaled inverse Fourier transform," *IEEE Journal of Selected Topics in Applied Earth Observations & Remote Sensing*, vol. 8, no. 3, pp. 1108–1119, 2015.

[21] J. Zheng, T. Su, H. Liu, G. Liao, Z. Liu, and Q. H. Liu, "Radar high-speed target detection based on the frequency-domain deramp-keystone transform," *IEEE Journal of Selected Topics in Applied Earth Observations and Remote Sensing*, vol. 9, no. 1, pp. 285–294, 2016.

[22] Z. Sun, X. Li, W. Yi, G. Cui, and L. Kong, "A coherent detection and velocity estimation algorithm for the high-speed target based on the modified location rotation transform," *IEEE Journal of Selected Topics in Applied Earth Observations and Remote Sensing*, vol. 11, no. 7, pp. 2346–2361, 2018.

[23] J. Su, M. Xing, G. Wang, and Z. Bao, "High-speed multi-target detection with narrowband radar," *IET Radar, Sonar & Navigation*, vol. 4, no. 4, pp. 595–603, 2010.

[24] X. Li, G. Cui, W. Yi, and L. Kong, "Manoeuvring target detection based on keystone transform and Lv's distribution," *IET Radar, Sonar & Navigation*, vol. 10, no. 7, pp. 1234–1242, 2016.

[25] X. Rao, H. Tao, J. Su, J. Xie, and X. Y. Zhang, "Detection of constant radial acceleration weak target via IAR-FRFT," *IEEE Transactions on Aerospace and Electronic Systems*, vol. 51, no. 4, pp. 3242–3253, 2015.

[26] X. Huang, L. Zhang, S. Li, and Y. Zhao, "Radar high speed small target detection based on keystone transform and linear

canonical transform," *Digital Signal Processing*, vol. 82, pp. 203–215, 2018.

[27] X. Li, Z. Sun, W. Yi, G. Cui, and L. Kong, "Radar detection and parameter estimation of high-speed target based on MART-LVT," *IEEE Sensors Journal*, vol. 19, no. 4, pp. 1478–1486, 2019.

[28] M. Xing, J. Su, G. Wang, and Z. Bao, "New parameter estimation and detection algorithm for high speed small target," *IEEE Transactions on Aerospace and Electronic Systems*, vol. 47, no. 1, pp. 214–224, 2011.

[29] X. Li, G. Cui, W. Yi, and L. Kong, "Coherent integration for maneuvering target detection based on Radon-Lv's distribution," *IEEE Signal Processing Letters*, vol. 22, no. 9, pp. 1467–1471, 2015.

[30] X. Lv, G. Bi, C. Wan, and M. Xing, "Lv's distribution: principle, implementation, properties, and performance," *IEEE Transactions on Signal Processing*, vol. 59, no. 8, pp. 3576–3591, 2011.

[31] J. Tian, W. Cui, Q. Shen, Z. Wei, and S. Wu, "High-speed maneuvering target detection approach based on joint RFT and keystone transform," *Science China Information Sciences*, vol. 56, no. 6, pp. 1–13, 2013.

[32] K. Jin, T. Lai, Y. Wang, G. Li, and Y. Zhao, "Coherent integration for radar high-speed maneuvering target based on frequency-domain second-order phase difference," *Electronics*, vol. 8, no. 3, p. 287, 2019.

[33] J. Tian, W. Cui, X.-G. Xia, and S.-L. Wu, "Parameter estimation of ground moving targets based on SKT-DLVT processing," *IEEE Transactions on Computational Imaging*, vol. 2, no. 1, pp. 13–26, 2016.

[34] K. Jin, T. Lai, S. Zhu, G. Li, T. Jin, and Y. Zhao, "Coherent detection and parameter estimation for radar high-speed maneuvering target based on FAF-LVD," *Circuits, Systems, and Signal Processing*, 2019.

[35] J. Tian, W. Cui, and S. Wu, "A novel method for parameter estimation of space moving targets," *IEEE Geoscience and Remote Sensing Letters*, vol. 11, no. 2, pp. 389–393, 2014.

[36] J. Xu, X. G. Xia, S. B. Peng, J. Yu, Y.-N. Peng, and L.-C. Qian, "Radar maneuvering target motion estimation based on generalized radon-Fourier transform," *IEEE Transactions on Signal Processing*, vol. 60, no. 12, pp. 6190–6201, 2012.

[37] W. Cui, J. Tian, X. G. Xia, and S. L. Wu, "An approach for parameter estimation of maneuvering targets with non-linear motions," *IEEE Transactions on Aerospace & Electronic Systems*, 2019.

[38] X. Li, G. Cui, W. Yi, and L. Kong, "A fast maneuvering target motion parameters estimation algorithm based on ACCF," *IEEE Signal Processing Letters*, vol. 22, no. 3, pp. 270–274, 2015.

[39] X. Li, G. Cui, L. Kong, and W. Yi, "Fast non-searching method for maneuvering target detection and motion parameters estimation," *IEEE Transactions on Signal Processing*, vol. 64, no. 9, pp. 2232–2244, 2016.

[40] X. Li, G. Cui, W. Yi, and L. Kong, "Fast coherent integration for maneuvering target with high-order range migration via TRT-SKT-LVD," *IEEE Transactions on Aerospace and Electronic Systems*, vol. 52, no. 6, pp. 2803–2814, 2016.

[41] X. Li, L. Kong, G. Cui, and W. Yi, "A low complexity coherent integration method for maneuvering target detection," *Digital Signal Processing*, vol. 49, pp. 137–147, 2016.

[42] J. Zheng, T. Su, L. Zhang, W. Zhu, and Q. H. Liu, "ISAR imaging of targets with complex motion based on the chirp rate–quadratic chirp rate distribution," *IEEE Transactions on Geoscience and Remote Sensing*, vol. 52, no. 11, pp. 7276–7289, 2014.

[43] P. O'Shea, "A fast algorithm for estimating the parameters of a quadratic FM signal," *IEEE Transactions on Signal Processing*, vol. 52, no. 2, pp. 385–393, 2004.

[44] J. Su, H.-H. Tao, X.-L. Guo, J. Xie, and X. Rao, "Coherently integrated cubic phase function for multiple LFM signals analysis," *Electronics Letters*, vol. 51, no. 5, pp. 411–413, 2015.

[45] J. Zheng, H. Liu, Z. Liu, and Q. Liu, "ISAR imaging of ship targets based on an integrated cubic phase bilinear autocorrelation function," *Sensors*, vol. 17, no. 3, p. 498, 2017.

[46] J. Zheng, H. Liu, J. Liu, X. Du, and Q. H. Liu, "Radar high-speed maneuvering target detection based on three-dimensional scaled transform," *IEEE Journal of Selected Topics in Applied Earth Observations and Remote Sensing*, vol. 11, no. 8, pp. 2821–2833, 2018.